Sposito, G. 1981b. The thermodynamics of soil solution. Clarendon Press, Oxford.
Sposito, G., and P. Fletcher. 1985. Sodium-calcium-magnesium exchange reactions on a montmorillonitic soil: III. Calcium-magnesium exchange selectivity. Soil Sci. Soc. Am. J. 49:1160–1163.
Sposito, G.K.L. Holtzclaw, C.T. Johnston, and C.S. LeVesque-Madore. 1981. Thermodynamics of sodium-copper exchange on Wyoming bentonite at 298 K. Soil Sci. Soc. Am. J. 45:1079–1084.
Sposito, G., and C.S. LeVesque. 1985. Sodium-calcium-magnesium exchange on silver Hill Illite. Soil Sci. Soc. Am. J. 49:1153–1159.
Sposito, G., C.S. LeVesque, and D. Hesterberg. 1986. Calcium-magnesium exchange on illite in the presence of adsorbed sodium. Soil Sci. Soc. Am. J. 50:905–909.
Sposito, G., K.M. Holtclaw, C.T. Johnston, and C.S. Le Vesque-Modore. 1981. Thermodynamics of sodium-copper exchange on Wyoming bentonite at 298 K. Soil Sci. Soc. Am. J. 45:1079–1084.
Sposito, G., K.M. Holtzclaw, C. Jonany, and L. Charlet. 1983. Cation selectivity in sodium-calcium, sodium-magnesium, and calcium-magnesium exchange on Wyoming bentonite at 298 K. Soil Sci. Soc. Am. J. 47:51–56.
Vanselow, A.P. 1932. Equilibria of the base-exchange reactions of bentonites, permutites, soil colloids, and zeolites. Soil Sci. 33:25–43.
Zhang, Z.Z., and D.L. Sparks. 1996. Sodium-copper exchange on Wyoming montmorillonite in chloride, perchlorate, nitrate, and sulfate solutions. Soil Sci. Soc. Am. J. 60:1750–1757.

Solid State ^{31}Phosphorus Nuclear Magnetic Resonance of Iron-, Manganese-, and Copper-Containing Synthetic Hydroxyapatites

B. Sutter,* R. E. Taylor, L. R. Hossner, and D. W. Ming

ABSTRACT

The incorporation of micronutrients into synthetic hydroxyapatite (SHA) is proposed for slow release of these nutrients to crops in the National Aeronautics and Space Administration's (NASA's) Advanced Life Support (ALS) program for Lunar or Martian outposts. Solid state ^{31}P nuclear magnetic resonance (NMR) was utilized to examine the paramagnetic effects of Fe^{3+}, Mn^{2+}, and Cu^{2+} to determine if they were incorporated into the SHA structure. Separate Fe^{3+}, Mn^{2+}, and Cu^{2+} containing SHA materials along with a transition metal free SHA (pure-SHA) were synthesized using a precipitation method. The proximity (<1 nm) of the transition metals to the ^{31}P nuclei of SHA were apparent when comparing the integrated ^{31}P signal intensities of the pure-SHA (87 arbitrary units g^{-1}) with the Fe-, Mn-, and Cu-SHA materials (37–71 arbitrary units g^{-1}). The lower integrated ^{31}P signal intensities of the Fe-, Mn-, and Cu-SHA materials relative to the pure-SHA suggested that Fe^{3+}, Mn^{2+}, and Cu^{2+} were incorporated in the SHA structure. Further support for Fe^{3+}, Mn^{2+}, and Cu^{2+} incorporation was demonstrated by the reduced spin-lattice relaxation constants of the Fe-, Mn-, and Cu-SHA materials (T' = 0.075–0.434 s) relative to pure-SHA (T_1 = 58.4 s). Inversion recovery spectra indicated that Fe^{3+}, Mn^{2+}, and Cu^{2+} were not homogeneously distributed about the ^{31}P nuclei in the SHA structure. Extraction with diethylene-triamine-penta-acetic acid (DTPA) suggested that between 50 and 80% of the total starting metal concentrations were incorporated in the SHA structure. Iron-, Mn-, and Cu-containing SHA are potential slow release sources of Fe, Mn, and Cu in the ALS cropping system.

The National Aeronautics and Space Administration's ALS program is currently evaluating crop production systems for Lunar or Martian outposts. Crops grown will minimize resupply costs from Earth by providing food and recycling air and water (Averner, 1989; Allen et al., 1995). The ALS program is developing a zeoponic-based plant growth system which is composed of a slow release fertilizer that combines an ammonium (NH_4^+) and potassium (K^+) charged clinoptilolite (zeolite) with a nutrient containing SHA [$Ca_{10}(PO_4)_6(OH)_2$] (Golden and Ming, 1999; Steinberg et al., 2000). Synthetic hydroxyapatite is produced to contain plant essential nutrients (Mg, Fe, Mn, Cu, Zn, S, Cl, Mo, and B) within the SHA structure. If nutrients can be incorporated into the structure of the sparingly soluble SHA, then slow-nutrient release from SHA at rates suitable for plant growth would be expected. This would be ideal for missions expected to last >1 yr.

Past research using x-ray diffraction (XRD) and infrared (IR) spectroscopy has determined that Fe, Mn, and Cu were substituted into the SHA structure (Tripathy et al., 1989; Golden and Ming, 1999). Golden and Ming (1999) noted that the d[002] spacing of the Fe^{2+}, Mn^{2+}, and Cu^{2+} substituted SHA was less than the unsubstituted SHA. Substitution of Cu^{2+} into SHA caused the *a* and *c* axes of the Cu^{2+} substituted SHA to be less than the unsubstituted SHA (Tripathy et al., 1989). Tripathy et al. (1989) and Golden and Ming (1999) reported the PO_4-ν_3 absorption wavenumber of the metal substituted SHA to be lower and higher, respectively, than the unsubstituted SHA.

This research examined a lower concentration range of transition metals (7–25 g kg^{-1}) in SHA than were studied by Tripathy et al. (1989, 66–512 g kg^{-1}) and Golden and Ming (1999, 15–50 g kg^{-1}). X-ray analyses of the transition metal containing SHA (metal-SHA) materials of this study did not show any x-ray lines that shifted relative to pure-SHA (Sutter, 2000). The low concentration of metals in SHA did not allow for significant shift of x-ray lines that would indicate incorporation of the metals in SHA. While IR was successful in detecting Fe and Mn incorporation into SHA, IR analyses did not indicate Cu incorporation into SHA (Sutter, 2000). The amount of Cu incorporated into SHA may have been too low for IR to detect. An analytical technique was required that could detect Fe, Mn, as well as Cu incorporation into SHA for the entire metal concentration range of this research. Solid state ^{31}P NMR spec-

B. Sutter, National Research Council, NASA, Ames Research Center, Moffett Field, CA 94035; R.E. Taylor, Dep. of Chemistry, and L.R. Hossner, Dep. of Soil and Crop Sciences, Texas A&M Univ., College Station, TX 77843; D.W. Ming, NASA Johnson Space Center, Houston, TX 77058. *Corresponding author (bsutter@mail.arc.nasa.gov).

Published in Soil Sci. Soc. Am. J. 66:455–463 (2002).

Abbreviations: ALS, Advanced Life Support; DTPA, diethylene-triamine-penta-acetic acid; IR, infrared; NASA, National Aeronautics and Space Administration; NMR, nuclear magnetic resonance; SHA, synthetic hydroxyapatite; XRD, x-ray diffraction.

troscopy proved an excellent analytical tool in detecting the incorporation of Fe, Mn, and Cu into the metal-SHA materials.

Solid state NMR can characterize the chemical environment of ^{31}P nuclei through information obtained from the spectral line shape and from the NMR relaxation parameters. When cross-polarization procedures were used, an increased number of spinning sidebands of ^{31}P magic angle spinning NMR resonances occurred that indicated the existence of HPO_4^{2-} in SHA and other synthetic calcium phosphates (Age et al., 1984; Roberts et al., 1991; Wu et al., 1994). However, ^{31}P NMR has not been used to examine the incorporation of the paramagnetic ions, Fe^{3+}, Mn^{2+}, and Cu^{2+} into the SHA structure. The presence of paramagnetic species complicates the examination of spinning sidebands for information on the chemical environment of the nucleus. Paramagnetic species can also give rise to spinning sidebands due to large magnetic susceptibility broadenings (Drain, 1962; Oldfield et al., 1983; Schroeder et al., 1998) in addition to any sidebands arising from the chemical shift anisotropy of the powdered sample.

The best approach to determine if Fe^{3+}, Mn^{2+}, and Cu^{2+} were incorporated into SHA is to examine the effect that Fe^{3+}, Mn^{2+}, and Cu^{2+} have on the ^{31}P relaxation parameters. Nuclear relaxation by paramagnetic species has long been known (Bloembergen, 1949). Solid state NMR has been used to illustrate that Fe^{3+} substituting for Al^{3+} in kaolinite and illite caused reductions of the ^{27}Al and ^{29}Si spin lattice relaxation time constants (T_1) relative to lower Fe^{3+}–containing kaolinite and illite (Hayashi et al., 1992; Shroeder and Pruett, 1996; Roch et al., 1998). Decreases in T_1 were due to the relaxation effects of the unpaired electrons from the substituted Fe^{3+}.

Spin-lattice relaxation occurs when the nuclear spin is perturbed by a radio frequency pulse and then relaxes or returns to equilibrium by interacting with its surroundings or lattice, resulting in a loss of energy (Sanders and Hunter, 1993). Spin-lattice relaxation is characterized by using a time-dependent equation of the following form:

$$M_t = M_o[1 - a \times \exp(-t/T_1)b] \quad [1]$$

where M_t is the magnetization at time t, M_o is the magnetization at equilibrium, t is time in seconds, T_1 is the spin-lattice time constant in seconds, and b is the exponent of the argument (Sanders and Hunter, 1993). The parameter a compensates for radio frequency inhomogeneity caused by the design of the probe, and can be estimated from the ratio of the initial magnetization and the M_o from the inversion recovery experiment. When nuclei are abundant (e.g., ^{19}F or ^{31}P) and spin-diffusion is present, relaxation follows exponential recovery (i.e., $b = 1$). In magnetically dilute nuclear systems (e.g., ^{29}Si or ^{13}C), nuclei cannot sense each other because they are too far apart; therefore, spin-diffusion does not occur. These nuclei will typically relax very slowly unless some other relaxation mechanism is present. For example,, the presence of paramagnetic species will cause these dilute nuclei to relax much faster and will be described by a nonexponential equation with $b = 0.5$ (Blumberg, 1960; Hayashi et al., 1992; Hartman et al., 1994). When $b \neq 1$, then T_1 is referred to as T' because T_1 is a well-known constant for exponential decay processes only (Hartman and Sherriff, 1991; Sanders and Hunter, 1993). When systems have magnetically abundant nuclear systems (e.g., ^{31}P) with paramagnetic centers, spin-diffusion and paramagnetic relaxation processes occur simultaneously, and b will range between 0.5 and 1 (Rorschach, 1964; Lowe and Gade, 1967; Lowe and Tse, 1968; Lewis et al., 1993).

The distance of a paramagnetic ion from the NMR active nucleus (e.g., ^{31}P) also has a role in the time required for relaxation. The farther the paramagnetic ion is away from the ^{31}P nucleus the less effect it will have on relaxing the ^{31}P nucleus. The relaxation rate decreases at a rate of r^{-6}, where r is the distance of the paramagnetic ion from the nucleus. If the distance between the ^{31}P and paramagnetic ion is doubled, then the relaxation rate will decrease by a factor of 64 (Sanders and Hunter, 1993). If the nucleus is too close to the paramagnetic species, then relaxation is so rapid that no signal is observed due to severe line broadening and frequency shift (Blumberg, 1960; Shroeder and Pruett, 1996). This has been described as the "wipeout sphere" model, where Fe^{3+} substituted on a regularly ordered basis for Al in kaolinite and eliminated any ^{27}Al NMR signal within a given radius of Fe^{3+} (Schroeder and Pruett, 1996). The loss of signal due to nuclei (<1 nm) close to the paramagnetic species has the effect of reducing the overall integrated signal intensity (Schroeder and Pruett, 1996). Therefore, if identical data acquisition conditions are used and there are no undetected species, materials without paramagnetic species will have larger integrated signal intensity than materials with paramagnetic species.

The overall goal of NASA's ALS program is to have a fundamental understanding of the incorporation of micronutrients into SHA and determine how useful SHA will be in supplying micronutrients to plants. This research produced singly incorporated transition metals to begin the process of examining micronutrient incorporation into SHA. The objective of this research was to utilize solid state ^{31}P NMR to determine if Fe^{3+}, Mn^{2+}, and Cu^{2+} were incorporated into the structure of SHA. Specifically, transition metal free SHA (pure-SHA), separate transition metal phases mixed with pure-SHA, and Fe^{3+}–, Mn^{2+}–, and Cu^{2+}–containing SHA will all be compared on the basis of (i) their integrated intensities of the ^{31}P signal, (ii) spectral characteristics, and (iii) their spin-lattice relaxation (T_1 and T') behavior.

MATERIALS AND METHODS

Pure-SHA was synthesized by a procedure similar to Golden and Ming (1999). Calcium nitrate [$Ca(NO_3)_2{\cdot}H_2O$] (235 g) was dissolved in 420 mL of 20% (v/v) NH_4OH while $(NH_4)_2HPO_4$ (72.2 g) was dissolved in 380 mL of deionized water. After the $(NH_4)_2HPO_4$ was completely dissolved, 30 mL of 20% (v/v) NH_4OH was added. The P solution was combined with the Ca solution and mixed by a propeller stirrer for 24 h. After mixing, the precipitate was allowed to age for 48 h. Subsequently, the NH_4OH solution was decanted and 2.5 L of deionized water was added. The SHA precipitate was mixed in water to dilute the NH_4OH and NO_3^- and then al-

Table 1. Total amounts of starting materials used as transition metal sources in hydroxyapatite synthesis, total elemental concentration of the synthetic hydroxyapatite (SHA) materials, and transition metal concentration in SHA after being treated with diethylene-triamine-penta-acetic acid (DTPA) for 2 and 4 h.

SHA material†	Transition metal source	Amount utilized	Elemental concentration				DTPA extracted	
			Ca	P	S	Metal	2h	4h
		g 100 mL^{-1}	g kg^{-1}					
Pure	–	–	380	179	–	–	–	–
Fe12	$Fe(NH_4)_2(SO_4)_2{\cdot}6H_2O$	8.244	362	179	9	12(Fe)‡	11(Fe)	8(Fe)
Fe25	$Fe(NH_4)_2(SO_4)_2{\cdot}6H_2O$	17.175	347	178	9	25(Fe)	23(Fe)	20(Fe)
Mn11	$MnSO_4{\cdot}H_2O$	3.557	366	178	6	11(Mn)	8(Mn)	7(Mn)
Mn24	$MnSO_4{\cdot}H_2O$	7.428	350	177	8	24(Mn)	15(Mn)	13(Mn)
Cu12	$Cu(NO_3)_2{\cdot}2.5H_2O$	4.880	370	181	–	12(Cu)	8(Cu)	7(Cu)
Cu20	$Cu(NO_3)_2{\cdot}2.5H_2O$	10.188	370	179	–	20(Cu)	12(Cu)	10(Cu)

† Numerals associated with each transition metal SHA are the concentrations (g kg^{-1}) of the transition metal in SHA before DTPA treatment.
‡ Metals in parentheses indicate which metal concentration was determined.

lowed to settle. The solution was then decanted. The washing procedure to remove excess NH_4OH and NO_3^- was repeated three more times. After washing, the apatite precipitate was separated from solution by filtering through a Whatman no. 41 filter paper. The pure-SHA precipitate was then put into an oven and heated at 400 °C for 24 h.

The transition metals were incorporated into SHA by dissolving the amounts of the transition metal materials listed in Table 1 in 100 mL of deionized water. The lowest Fe addition was based on the Fe addition used by Golden and Ming (1999) in synthesizing nutrient-substituted carbonate hydroxyapatite. Similar levels of Mn and Cu were used so the NMR analyses could compare all three metal contents. Higher Fe, Mn, and Cu additions were used to examine how T' would change with increased metal concentration. The metal solution was then added to the P solution and mixed for 5 min. The metal/P solution was then added to the Ca solution, and the remaining procedure was followed as outlined above. A total of six transition metal containing SHA (Table 1) and one pure-SHA were synthesized. When referring to the six transition metal containing SHA collectively, they will be termed metal-SHA. Numbers associated with the metal-SHA labels are their approximate concentration (g kg^{-1}) in SHA. All SHA materials were ground to pass through a 45-μm sieve. Iron(III) dominated in Fe-SHA on the basis of the yellow coloration of these materials and electron paramagnetic resonance spectroscopy analyses (Sutter, 2000). Manganese(II) prevailed in the Mn-SHA materials due to their pink coloring.

Total Ca, P, S, Fe, Mn, and Cu analyses were performed with a Cameca SX-50 electron microprobe. The SHA materials were pressed into pellets (103.5 MPa) and analyzed at 15 kV and 10 nA with a beam diameter of 20 μm. The electron microprobe sample stage was moved back and forth at 20-μm steps across a length of 200 μm to obtain an average chemical analysis. Polished C.M. Taylor (Gold Beach, OR) and the Smithsonian standards were used in calibrating the electron microprobe. X-ray diffraction analyses of the SHA materials were conducted with a Rigaku 200 powder diffractometer (Tokyo, Japan). Copper Kα x-rays were produced from a rotating anode at 50 kV and 180 mA. A step size of 0.02° for 10 s was performed in the range of 10 to 100° 2θ.

Diethylene-triamine-penta-acetic acid complexes with soluble and exchangeable Fe, Mn, and Cu, as well as mobilize these metals from Fe-, Mn-, and Cu-containing solid phases [e.g., metal-oxyhydroxides] (Loeppert and Inskeep, 1996). Each metal-SHA was treated with a DTPA solution to determine if the nonstructural transition metal phases detected by electron paramagnetic resonance analyses (Sutter, 2000) could affect the ^{31}P spectra or the ^{31}P relaxation rate. The Fe12-, Fe25-, Mn11-, Mn24-, Cu12-, and Cu20-SHA materials (0.1 g) were exposed to 35 mL of 0.001 *M* DTPA for 2 h on a reciprocating shaker. Subsequently, the SHA materials were centrifuged at 1271 G for 3 min and the solution decanted and filtered though 0.2-mm filter paper. Iron, Mn, and Cu solution concentrations were determined with a Perkin Elmer 3100 flame atomic absorption spectrometer (Norwalk, CT). The SHA materials were washed by adding 35 mL of deinoized water and shaken for 10 min followed by centrifugation; the washing process was repeated one more time. The SHA samples were air dried at 65 °C and then examined by ^{31}P NMR. For another set of samples the above process was repeated, therefore exposing the SHA materials to DTPA for a total of 4 h. Total Fe, Mn, and Cu in the extracting solution was subtracted from starting concentration of Fe, Mn, and Cu in the metal-SHA materials to determine remaining Fe, Mn, and Cu concentrations in the metal-SHA materials.

Magic angle spinning solid state ^{31}P NMR was performed on a Fourier transform Bruker (Billerica, MA) MSL 300 NMR spectrometer at room temperature (297 K). The ^{31}P signal at 121 MHz was referenced to 85% (v/v) phosphoric acid (H_3PO_4). Qualitative ^{31}P spectra were obtained (spin frequency 2.0 kHz) for all SHA materials to assess the spinning sideband character of the SHA spectra. Quantitative (integrated intensities) ^{31}P NMR data (spin rate 4.55 kHz) were acquired for the pure-, Fe12-, Mn11-, and Cu12-SHA materials. One percent by weight of ferrihydrite (two line, $5Fe_2O_3{\cdot}9H_2O$) $MnSO_4{\cdot}H_2O$, $MgSO_4$, and $Cu(NO_3)_2{\cdot}2.5H_2O$ were separately mixed with pure-SHA to determine the effect of these separate phases on the integrated intensity of the ^{31}P signal relative to the pure-, Fe12-, Mn11-, and Cu12-SHA materials. The mixed phases were produced to simulate the occurrence of metal phases that might have precipitated separately from the metal-SHA materials. The ferrihydrite, $MnSO_4{\cdot}H_2O$, $MgSO_4$, and $Cu(NO_3)_2{\cdot}2.5H_2O$ phases mixed with pure-SHA were labeled as Fe-mix, Mn-mix, Mg-mix, and Cu-mix, respectively. The qualitative and quantitative ^{31}P spectra (including all observed sidebands) were acquired with a π/2 excitation pulse with $5 \times T_1$ between scans. Acquisition time was 80 ms for each scan. Sample size was 300 mg. Sixteen scans were used for the pure-SHA and mixed phases. The Fe-, Mn-, and Cu-SHA materials had a lower signal:noise ratio than pure-SHA and therefore required 64 scans.

Inversion recovery experiments were performed using a standard π–τau–π/2 radio frequency pulse sequence (π/2 pulse width was 4 μs), where τau is the time (s) of variable delay to determine T_1 or T' of all SHA and mixed pure-SHA materials. Samples were spun at a frequency of 4.55 kHz. Nonlinear least-squares analysis was used to fit the exponential (T_1 and $b = 1$) and nonexponential ($T'$and $b \neq 1$) equations (Eq. [1]) to the plots of magnetization vs. the time between the π and

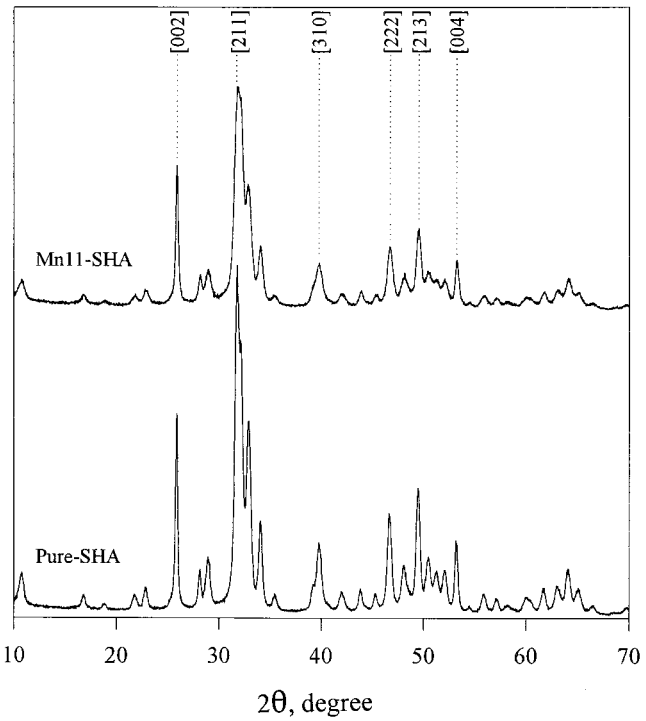

Fig. 1. X-ray diffraction patterns of pure-synthetic hydroxyaptite (SHA) and Mn11-SHA with the primary SHA diffraction peaks (hkl) labeled.

π/2 pulse (variable delay) (Jandel Scientific, 1994). The T_1 or T' values were allowed to vary while the b values were manually varied until the best fit was obtained. The M_o and a values were fixed.

RESULTS

Total Chemical Analysis and X-Ray Diffraction

The detected amounts of Fe, Mn, and Cu in their respective SHA materials are in Table 1. X-ray diffraction plots of pure-SHA and Mn11-SHA have (hkl) reflections characteristic of apatite (Fig. 1). The Mn24-, Fe12-, Fe25-, Cu12-, and Cu20-SHA XRD patterns (not shown) also possessed the characteristic (hkl) reflections of apatite. The Mn11-SHA along with the other metal-SHA materials exhibited increased peak broadening relative to pure-SHA. Increased strain and decreased particle size of the metal-SHA materials relative to pure-SHA caused the XRD peak broadening observed with the metal-SHA materials (Sutter, 2000).

^{31}Phosphorus Nuclear Magnetic Resonance

The 2 kHz ^{31}P spectra of the pure-SHA, Cu12-, and Cu20-SHA and the Mg-mix and Cu-mix materials (Fig. 2a,b) all had four small spinning sidebands. The Fe-mix, Mn-mix, Fe12-, Fe25-, Mn11-, and Mn24-SHA had a greater number of spinning sidebands relative to pure-SHA (Fig. 2a,b). Isotropic ^{31}P chemical shifts values for all SHA materials were 2.6 ± 0.2 mg kg^{-1}. This

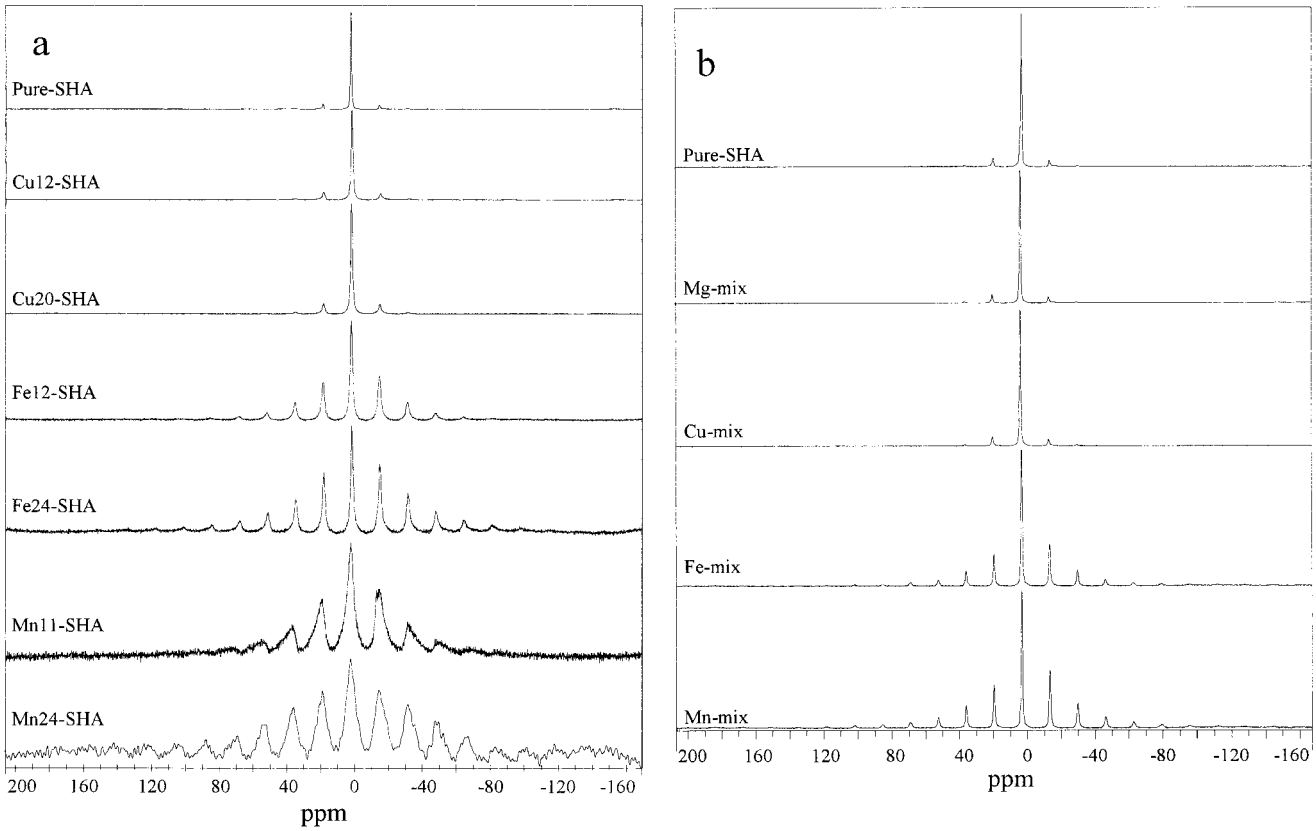

Fig. 2. ^{31}Phosphorus NMR spectra (2.0 kHz spin frequency) of: (a) pure-, Cu12-, Cu20-, Fe12-, Fe25-, Mn11-, and Mn24-synthetic hydroxyapatite (SHA); and (b) pure-SHA and pure-SHA mixed with 1.0 wt.% of $MnSO_4$·H_2O (Mn-mix), ferrihydrite ($5Fe_2O_3$·$9H_2O$) (Fe-mix), $Cu(NO_3)_2$·$2.5H_2O$ (Cu-mix), and $MgSO_4$ (Mg-mix). Spectral intensities were scaled for ease of comparison.

corresponds well with SHA literature values of 2.8 mg kg^{-1} (Age et al., 1984; Wu et al., 1994). The concentration in the metal-SHA materials was too low to cause a significant isotropic shift.

No major differences between the integrated intensities of the Mg-mix, Fe-mix, Mn-mix, and Cu-mix materials and pure-SHA were observed (Table 2). However, the integrated intensities of the Fe12-, Mn11-, and Cu12-SHA were lower than the integrated intensities of the pure-SHA and all the mixed materials (Table 2).

Inversion recovery spectra for pure-SHA (Fig. 3a) were similar to the inversion recovery spectra of the mixed materials (data not shown). The inversion recovery spectra of Mn11-SHA (Fig. 3b) and Fe12-, Fe25-, Mn24-, Cu12-, and Cu20-SHA (data not shown) were unlike pure-SHA near 0 magnetization. The spinning side bands of all the metal-SHA recovered before the central peak, and there were two shoulders on either side of the central peak similar to that observed for Mn11-SHA (Fig. 3b). Expansion of the three spectra nearest to zero magnetization during the recovery sequence indicated that the same phenomena observed for all the metal-SHA not treated by DTPA occurred for all the metal-SHA treated by DTPA (Fig. 4).

Plots of magnetization (M_t) vs. time (t) of the inversion recovery experiments indicated that pure-SHA and the Mn-mix (Fig. 5a) had slower ^{31}P relaxation than the metal-SHA and metal-SHA treated with DTPA (Fig. 5b,c). The magnetization of the metal-SHA and metal-SHA treated with DTPA samples reached equilibrium between t = 1 and 3 s. Pure-SHA and the Mn-mix materials required 300 s to reach equilibrium. The Mg-mix, Fe-mix and Cu-mix materials also required 300s to reach equilibrium (data not shown).

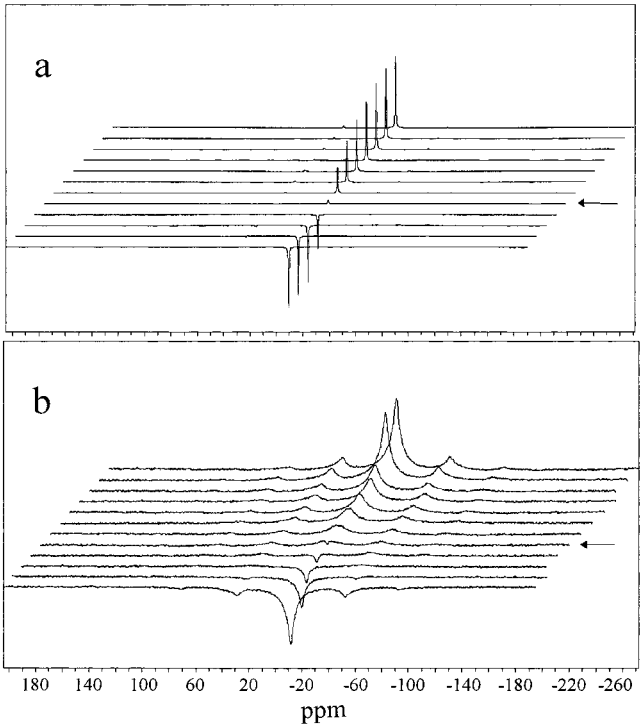

Fig. 3. Inversion recovery stacked ^{31}P spectra of: (a) pure-SHA and; (b) Mn11-SHA. Arrows indicate spectra closest to zero magnetization.

Table 2. ^{31}Phosphorus integrated signal intensities for pure-synthetic hydroxyapatite (SHA), SHA containing transition metals, and separate phases mixed with pure-SHA.

SHA material†	Integrated signal intensities
	arbitrary units g^{-1}‡
Ferrihydrite and pure-SHA (Fe-mix)	84
$Cu(NO_3)_2{\cdot}2.5H_2O$ and pure-SHA (Cu-mix)	92
$MnSO_4{\cdot}H_2O$ and pure-SHA (Mn-mix)	90
$MgSO_4$-and pure-SHA (Mg-mix)	90
Pure-SHA	87
Fe12-SHA	71
Cu12-SHA	63
Mn11-SHA	37

† Numerals associated with each transition metal SHA are the concentrations (g kg^{-1}) of the transition metal in SHA.

‡ Integrated signal intensity is a function of the applied magnetic field strength and scaling of the Fourier transformed signal which is controlled by the NMR operator; hence, arbitrary units g^{-1} are used. All ^{31}P integrated signal intensities were collected and Fourier transformed under identical conditions.

Magnetization vs. time plots of pure-SHA and the Mn-mix were best described by an exponential equation where b = 1.0 (Table 3). The Mg-mix, Fe-mix, and Cu-mix were also best described by the exponential equation and had parameters similar to pure-SHA (data not shown). All the metal-SHA and metal-SHA treated with DTPA were best described by a nonexponential equation where b ranged from 0.63 to 0.79 (Table 3). The T' for the metal-SHA samples and the metal-SHA treated with DTPA were all at least two orders of magni-

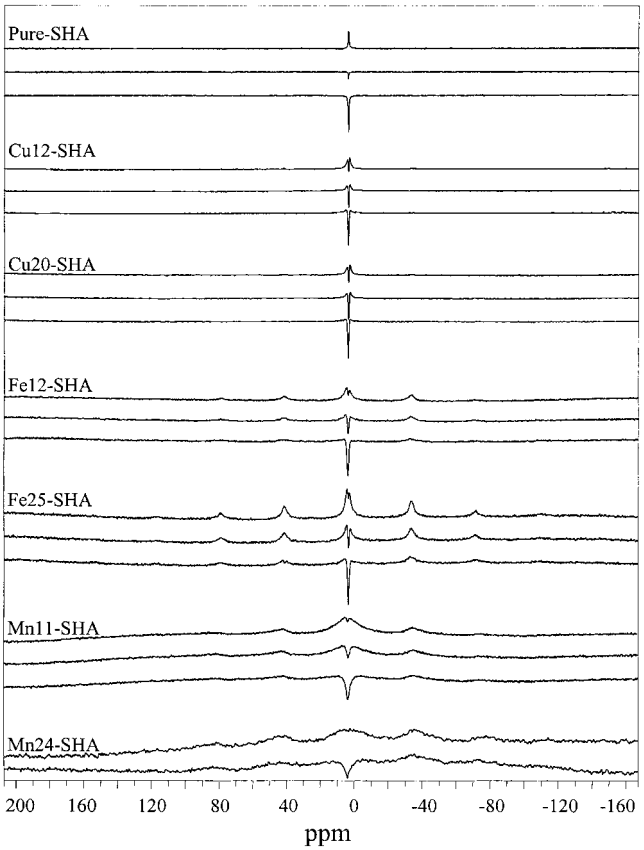

Fig. 4. ^{31}Phosphorus NMR signals passing through zero magnetization of pure-, Cu12-, Cu20-, Fe12-, Fe25-, Mn11- and Mn24-SHA after being treated 4 h with DTPA.

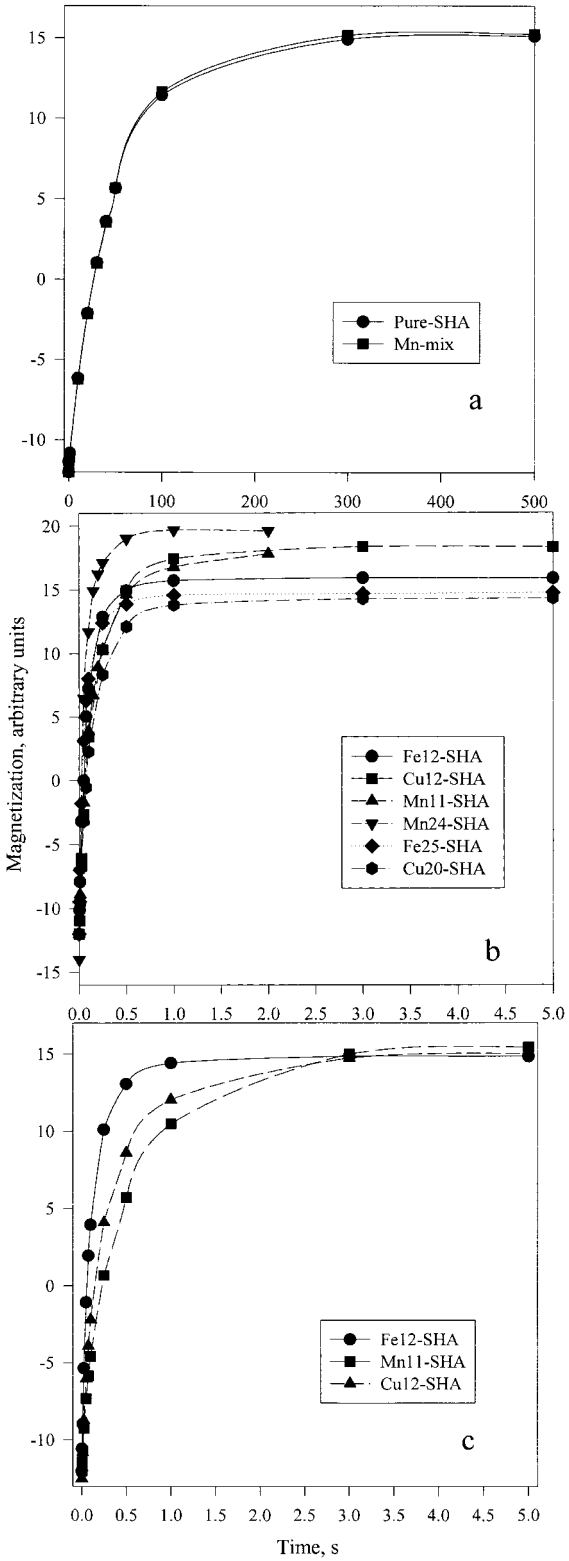

Fig. 5. ^{31}Phosphorus magnetization recovery curves as a function of time for: (a) pure synthetic hydroxyapatite (SHA) and the mixture of $MnSO_4 \cdot H_2O$ and pure-SHA (Mn-mix); (b) all the Metal-synthetic hydroxyapatites; and (c) Fe12-, Mn11-, and Cu12-SHA after being treated 4 h with DTPA.

tude less than the T_1 for pure-SHA and Mn-mix (Table 3). When the metal-SHA data were fitted exponentially ($b = 1$), T_1 values were similar to T' values (data not shown). The similarities between T_1 and T' for the metal-SHA and the large differences between T_1 of pure-SHA and T' of metal-SHA suggested that T_1 of pure-SHA could be safely compared with T' of the metal-SHA. The T' values were used to describe the metal-SHA because improved r^2 values were obtained when the nonexponential equation ($b \neq 1$, T') was used. T' increased as the metal concentration decreased with DTPA treatment (Table 3). The Fe12- and Fe25-SHA were the only materials that did not have greater T' after DTPA treatment.

Equation [1] has the exponential ($b = 1$) linear form of

$$\ln\frac{M_o - M_t}{M_o} = \frac{-1}{T_1}t + \ln a, \qquad [2]$$

where plotting

$$\ln \frac{M_o - M_t}{M_o}$$

vs. t should yield a straight line when spin-diffusion is the dominant process controlling spin-lattice relaxation. A plot of

$$\ln \frac{M_o - M_t}{M_o}$$

vs. t for pure-SHA was linear (Fig. 6a). The Fe12-SHA plot was linear at longer times (>0.2 s) and then deviated from linearity at shorter times (0–0.2 s) (Fig. 6b). For the Fe12-SHA plot, an exponential equation was used ($b = 1$) to demonstrate that the equation did not fit at shorter times for SHA containing paramagnetic species (Fig. 6b). The lack of fit at the shorter times for the metal-SHA was the reason the nonexponential equation had a better fit than the exponential equation.

DISCUSSION

The existence of spinning sidebands in the metal-SHA ^{31}P NMR spectra was anticipated to provide additional information on the chemical shift anisotropy, which is useful in characterizing chemical bonding. However, the presence of the multiple spinning side bands were also shown to occur in the Fe-mix and the Mn-mix materials and were attributed to magnetic susceptibility effects (Drain, 1962; Oldfield et al., 1983). Magnesium is diamagnetic, therefore, the Mg-mix spectrum did not have multiple spinning sidebands. The greater the number of unpaired electrons, the greater the magnetic susceptibility (Gerloch and Constable, 1994). Copper(II) has only one unpaired electron compared with Mn^{2+} and Fe^{3+} that have five unpaired electrons. Therefore, the Cu12- and Cu20-SHA and the Cu-mix materials had a lower number of spinning sidebands than the Mn- and Fe-SHA and Fe-mix and Mn-mix materials (Fig. 2a,b). The only effect magnetic susceptibility has on the ^{31}P NMR spectra is to increase the number of spinning side bands due to line broadening. Unlike paramagnetic effects, magnetic susceptibility need not affect integrated intensity, T_1, or T'.

Two factors together or separately can cause lower integrated intensities of the metal-SHA. The first is paramagnetic ions (Fe^{3+}, Mn^{2+}, and Cu^{2+}) incorporated

Table 3. Results of nonlinear least squares analyses of the magnetization equation $M_t = M_o\{1\text{-}a[\exp\text{-}(t/T_a)^b]\}$ for the untreated and the 2-h and 4-h diethylene-triamine-penta-acetic acid (DTPA) treated synthetic hydroxyapatite (SHA) materials. The spin-lattice constant, T_a, was T_1 for all samples containing pure-SHA, while T_a was T' for samples not containing Pure-SHA. The exponent b equals 1 when relaxation is controlled by spin diffusion, and ranges from 0.5 to <1 when spin diffusion and paramagnetic effects control relaxation. Coefficient of determination (r^2) ranged from 0.99 to 1.00 for all analyses.

	Synthetic hydroxyapatite							
Treatment	**Pure**	**Mn-mix**	**Fe12**	**Fe25**	**Mn11**	**Mn24**	**Cu12**	**Cu20**
	T_1		T'					
	s							
Untreated	**47.6**	**47.9**	**0.0819**	**0.0584**	**0.146**	**0.053**	**0.162**	**0.142**
2-h DTPA	**53.9**	**–**	**0.0760**	**–**	**0.297**	**–**	**0.248**	**–**
4-h DTPA	**58.4**	**–**	**0.0759**	**0.0554**	**0.434**	**0.279**	**0.302**	**0.324**
	b							
Untreated	**1.0**	**1.0**	**0.79**	**0.70**	**0.69**	**0.67**	**0.73**	**0.77**
2-h DTPA	**1.0**	**–**	**0.74**	**–**	**0.63**	**–**	**0.74**	**–**
4-h DTPA	**1.0**	**–**	**0.75**	**0.72**	**0.76**	**0.73**	**0.70**	**0.70**

into the SHA structure enhanced the relaxation of ^{31}P. The paramagnetic ions that were close (<1 nm) enough to the ^{31}P nuclei completely eliminated the ^{31}P signal, which contributed to a reduction in the integrated intensity (Schroeder and Pruett, 1996). The paramagnetic ions that were >1 nm from the ^{31}P nuclei reduced but did not eliminate the ^{31}P signal. The effect the paramagnetic ions have on the ^{31}P integrated intensity decreases as the distance from the ^{31}P nuclei increases (Sanders and Hunter, 1993; Schroeder and Pruett, 1996). The second factor is poorly crystalline metal phosphate that is associated with SHA. Poorly crystalline metal phases associated with SHA were detected by electron paramagnetic resonance spectroscopy and were likely to be poorly crystalline metal phosphate (Sutter, 2000). The abundance and closeness of paramagnetic ions to ^{31}P nuclei in the poorly crystalline metal phosphate did not allow for a ^{31}P signal to come from the poorly crystalline metal phosphate, thus causing overall lower integrated intensities in the metal-SHA/metal phosphate system (Blumberg, 1960; Hinedi et al., 1989; Shroeder and Pruett, 1996). The metal-mixed phases indicated that separate nonphosphate phases could not affect the integrated intensity of metal-SHA. The Fe-mix, Mn-mix, and Cu-mix materials did not affect the integrated intensity of the ^{31}P signal because Fe^{3+}, Mn^{2+}, and Cu^{2+} were too far away (i.e., r^{-6} dependence on relaxation) from any ^{31}P nucleus to enhance relaxation. The increased distance in the mixtures indicated that Fe^{3+}, Mn^{2+}, and Cu^{2+} were not part of the SHA structure.

The occurrence of shoulders on the central peak of the metal-SHA materials indicated the presence of two central peaks recovering at different rates. The combination of a faster recovering peak with a slower recov-

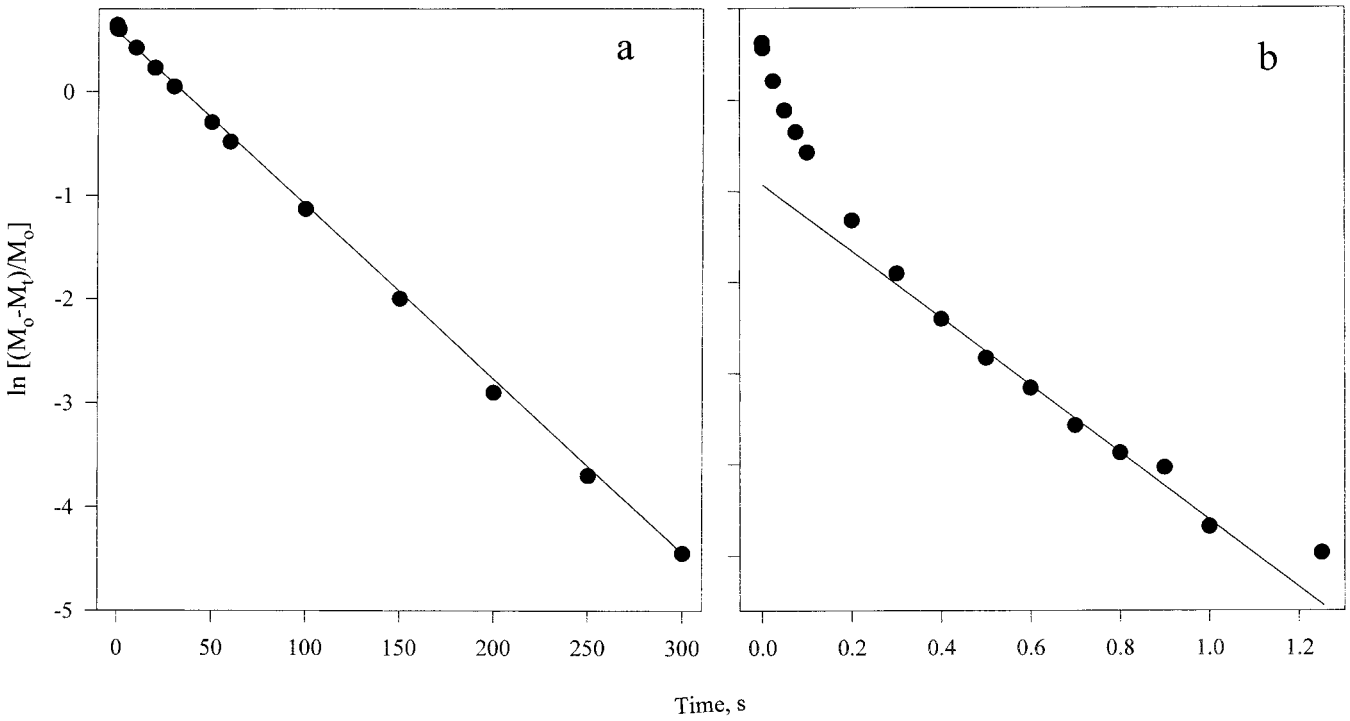

Fig. 6. The linearized form of the spin-lattice relaxation equation as a function of time for: (a) pure-SHA and (b) Fe12-SHA. The solid line indicated where spin-diffusion was controlling ^{31}P relaxation in pure-SHA and Fe12-SHA. Points that deviated from the solid line at early times in Fe12-SHA indicated where paramagnetic effects from Fe^{3+} were controlling ^{31}P relaxation.

ering peak caused the appearance of the shoulders on the overall central peak. The faster recovering peak is indicated by the shoulders that pass through zero magnetization before the slower recovering peak. The spinning sidebands that recovered before the two central peaks were associated with the faster recovering central peak. The existence of the two peaks could be described by two T' values which indicated the existence of two phosphorus environments relaxing at slightly different rates. One possibility is a heterogeneous concentration effect where one T' was due to higher local concentrations of paramagnetic ions near ^{31}P, while the other T' was due to a lower concentration of paramagnetic ions near ^{31}P. The occurrence of higher and lower concentrations of paramagnetics near ^{31}P would produce lower and higher T' values, respectively. Only one overall T' was determined for the metal-SHA because the difference between the two T' values was shown to be small by the observation only near zero magnetization. Poorly crystalline metal phosphate was proposed to cause the second peak. However, a second peak caused by a metal-phosphate phase is not possible because the abundance and closeness of paramagnetic species to the ^{31}P nuclei in a metal-phosphate is too great to allow for an observable ^{31}P signal (Blumberg, 1960; Hinedi et al., 1989; Schroeder and Pruett, 1996). This was proven with $FePO_4 \cdot H_2O$ which did not yield a ^{31}P signal (data not shown). Hinedi et al. (1989) also did not obtain a ^{31}P NMR spectra of Fe- and Mn-phosphate minerals because of strong paramagnetic effects.

The rapid magnetization recoveries of the metal-SHA and the metal-SHA treated with DTPA when compared with the pure-SHA indicated that the metals in those samples were incorporated close (<1 nm) to the ^{31}P nucleus, and must be part of the SHA structure. The Fe-mix, Mn-mix, and Cu-mix magnetization recoveries were similar to the pure-SHA recoveries, indicating that the separate metals phases in the metal-SHA could not be responsible for rapid magnetization recoveries observed in the metal-SHA samples. The rapid magnetization recovery of the metal-SHA materials also indicates that Fe, Mn, and Cu incorporated into the SHA structure were at least partly responsible for the reduced integrated signal intensity.

The metal-SHA data were best described with a non-exponential equation (b = 0.69–0.79). If b was to equal 0.5 for the metal-SHA, then ^{31}P relaxation would be due solely to paramagnetic effects (i.e., no spin diffusion). The range of b values between 0.69 to 0.79 indicated that both spin diffusion and paramagnetic effects were responsible for ^{31}P relaxation in the metal-SHA materials (Rorschach, 1964; Lowe and Gade, 1967; Lowe and Tse, 1968; Lewis et al., 1993). Spin diffusion was expected in all SHA materials because ^{31}P is a magnetically abundant species. Paramagnetic relaxation of ^{31}P nuclei would be expected if the paramagnetic ions (Fe^{3+}, Mn^{2+}, and Cu^{2+}) were incorporated into the SHA structure and near the ^{31}P nuclei on the order of 1 nm.

The lower T' values of the metal-SHA and the metal-SHA treated with DTPA relative to the T_1 of pure-SHA indicated that Fe^{3+}, Mn^{2+}, and Cu^{2+} were effective at reducing the relaxation time of ^{31}P. The reduced relaxation time provided further support that Fe^{3+}, Mn^{2+}, and Cu^{2+} were incorporated into the SHA structure and were within atomic scale distances of the ^{31}P nuclei.

As the concentration of the metals increased, the T' values decreased, indicating a T' dependence on metal concentration. The higher metal concentration caused more metals to interact closely with the P nuclei. This led to increased paramagnetic relaxation effects on the P nuclei, resulting in lower T' values.

The higher T_1 reported for pure-SHA with DTPA treatment was attributed to removal of paramagnetic impurities that were acquired from the reagents used to synthesize pure-SHA. No impurity effect would have been observed in the metal-SHA because the added paramagnetic ions dominated the relaxation process. The DTPA treatment was performed to see if any Fe^{3+}, Mn^{2+}, and Cu^{2+} were removed from SHA that might have affected the relaxation of the ^{31}P signal. The trend of increasing T' with DTPA treatment for the Mn- and Cu-SHA materials indicated that the DTPA removed Mn^{2+} and Cu^{2+} from the SHA structure, causing a reduction in the amount of Mn^{2+} and Cu^{2+} interacting with P. The reduction in the Mn^{2+} and Cu^{2+} concentration of SHA was confirmed by the concentrations of Mn^{2+} and Cu^{2+} being lower in SHA treated by DTPA than SHA not treated by DTPA (Table 1). Lower concentrations of Mn^{2+} and Cu^{2+} in the SHA decreased the paramagnetic relaxing effects on the P nuclei, causing T' to increase. While DTPA extracted structural metals from SHA, the removal of poorly crystalline metal phases associated with SHA also contributed to the decrease in the total starting metal concentrations. The difference between the 2- and 4-h DTPA extractions are not large, indicating that DTPA could not remove significantly more metal from SHA. The metals remaining after a 4-h treatment were metals strongly incorporated into the SHA structure. Examination of the 4-h DTPA metal concentration data suggests that between 50 and 80% of the total metals before DTPA extraction were incorporated into the SHA structure. Unlike the Mn- and Cu-SHA materials, T' for the Fe-SHA materials did not change significantly with DTPA treatment, despite the reduction of Fe concentration (Table 1). A possible explanation was that DTPA only extracted Fe not closely associated with P, and did not extract structural Fe that was closely associated with P. Nevertheless, T' values remained extremely low after all DTPA treatments for the metal-SHA, indicating that the transition metals were within the SHA structure and inaccessible to DTPA.

The linear plot of the exponential equation (b = 1) for pure-SHA was a near-perfect fit and supports the presence of spin diffusion throughout the entire relaxation period. The fit for the same linear exponential plot for Fe12-SHA fits the data well at times >0.2 s because spin-diffusion was the dominant relaxation process at the longer times. The linear exponential line deviated from linearity at times <0.2 s, indicating that direct dipolar coupling with the electron spin of the paramagnetic species was responsible for ^{31}P relaxation at the times <0.2 s (Hayashi et al., 1992). Paramagnetic relaxation was extremely rapid, and dominated at an early stage of the relaxation process (Blumberg, 1960).

CONCLUSION

The two processes that affected ^{31}P relaxation in the metal-SHA materials were spin-diffusion and paramagnetic effects. Spin-diffusion was due to the abundance of ^{31}P nuclei while the paramagnetic effects were due to the incorporation of Fe^{3+}, Mn^{2+}, and Cu^{2+} into SHA. The presence of paramagnetic impurities rendered the extraction of chemical bonding information difficult due to the problem of separating chemical shift anisotropy effects from magnetic susceptibility broadening. Hence, spin-lattice relaxation proved to be a better approach for showing that Fe^{3+}, Mn^{2+}, and Cu^{2+} were incorporated into the SHA structure. The range of b (0.63–0.79) for the metal-SHA materials supported the presence of spin-diffusion and paramagnetically controlled relaxation. The exponential fit at times >0.2 s in the metal-SHA supported the existence of spin-diffusion effects on ^{31}P relaxation. The low T' values, decreased integrated intensities of the ^{31}P spectra, and the lack of exponential fit at times <0.2 s supported paramagnetic effects on ^{31}P relaxation. The significantly lower integrated intensities of the ^{31}P NMR spectra and lower T' values of the metal-SHA relative to the pure-SHA indicated that Fe^{3+}, Mn^{2+}, and Cu^{2+} ions occurred near the ^{31}P nuclei on the order of 1 nm and were incorporated into the SHA structure.

Nuclear magnetic resonance spectroscopy cannot unequivocally prove that the Fe^{3+}, Mn^{2+}, and Cu^{2+} substituted for Ca^{2+} in the SHA. Nevertheless, the enhanced relaxation of the ^{31}P nuclei in metal-SHA indicated that Fe^{3+}, Mn^{2+} and Cu^{2+} were close to P on an atomic scale. The closeness of Fe^{3+}, Mn^{2+} and Cu^{2+} to P indicated bonding with phosphate, suggesting substitution of these transition metals into one or both of the Ca sites. The metal-substituted SHA materials will act as slow-release fertilizers of Fe, Cu, Mn, Ca, and P. The SHA materials could be used as a slow-release source of these elements in solid substrates used in the ALS cropping system, as well as terrestrial agriculture applications.

ACKNOWLEDGMENTS

This research was partially funded by NASA's Graduate Student Researchers Program (NGT 51229) in conjunction with Johnson Space Center, Houston, TX. The authors would like to thank Ray Guillemette for his assistance with electron microprobe analyses. The authors are grateful to Dr. Richard Morris, the three anonymous reviewers, and the associate editor Dr. Cliff Johnston for their critical review of this manuscript.

REFERENCES

Allen, E.R., D.W. Ming, L.R. Hossner, D.L. Henninger, and C. Galindo. 1995. Growth and nutrient uptake of wheat in clinoptilolite-phosphate rock substrates. Agron. J. 87:1052–1059.

Aue, W.P., A.H. Roufosse, M.J. Glimcher, and R.G. Griffen. 1984. Solid-state phosphorus-31 nuclear magnetic resonance studies of synthetic solid phases of calcium phosphate: Potential models of bone mineral. Biochemistry 23:6110–6114.

Averner, M.M. 1989. Controlled ecological life support systems p. 145–153. *In* D.W. Ming and D.L. Henninger (ed.) Lunar base agriculture: Soils for plant growth. ASA, CSSA, and SSSA, Madison, WI.

Bloembergen, N. 1949. On the interaction of nuclear spins in a crystalline lattice. Physica 15:386–426.

Blumberg, W.E. 1960. Nuclear spin-lattice relaxation caused by paramagnetic impurities. Phys. Rev. 119:79–84.

Drain, L.E. 1962. The broadening of magnetic resonance lines due to field inhomogeneities in powdered samples. Proc. Phys. Soc. 80:1380–1382.

Gerloch, M., and E.C. Constable. 1994. Transition metal chemistry. Verlagsgesellschaft mbH, Weinheim, Germany.

Golden, D.C., and D.W. Ming. 1999. Nutrient-substituted hydroxyapatites: Synthesis and characterization. Soil Sci. Soc. Am. J. 63:657–664.

Hartman, J.S., A. Narayanna, and Y. Wang. 1994. Spin-lattice relaxation in the 6H polytype of silicone carbide. J. Am. Chem. Soc. 116:4019–4027.

Hartman, J.S., and B.L. Sherriff. 1991. ^{29}Si MAS NMR of the aluminosilicate mineral kyanite: Residual dipolar coupling to ^{27}Al and non-exponential spin-lattice relaxation. J. Phys. Chem. 95:7575–7579.

Hayashi, S., T. Ueda, K. Hayamizu, and E. Akiba. 1992. NMR study of kaolinite. 2. ^{1}H, ^{27}Al, and ^{29}Si spin-lattice relaxations. J. Phys. Chem. 96:10928–10933.

Hinedi, Z.R., A.C. Chang, J.P. Yesinowski. 1989. Phosphorus-31 magic angle spinning nuclear magnetic resonance of wastewater sludges and sludge-amended soil. Soil Sci. Soc. Am. J. 53:1053–1056.

Jandel Scientific. 1994. SigmaStat Statistical Software for Windows. Version 1.0. Jandel Scientific, San Rafael, CA.

Lewis, R.H., R.A. Wind, and G.E. Maciel. 1993. Investigation of cured hydridopolysilazane-derived ceramic fibers via dynamic nuclear polarization. J. Mater. Res. 8:649–654.

Loeppert, R.H., and W.P. Inskeep. 1996. Iron. p. 639–664. *In* D.L. Sparks et al. (ed.) Methods of soil analysis. Part 3. SSSA Book Ser. 5. SSSA, Madison, WI.

Lowe, I.J., and S. Gade. 1967. Density-matrix derivation of the spin-diffusion equation. Phys. Rev. 156:817–825.

Lowe, I.J., and D. Tse. 1968. Nuclear spin-lattice relaxation via paramagnetic centers. Phys. Rev. 166:279–291.

Oldfield, E., R.A. Kinsey, K.A. Smith, J.A. Nichols, and J. Kirkpatrick. 1983. High-resolution NMR of inorganic solids. Influence of magnetic centers on magic-angle sample-spinning lineshapes in some natural aluminosilicates. J. Magn. Reson. 51:325–329.

Roberts, J.E., M. Heughebaert, J.C. Heughebaert, L.C. Bonar, M.J. Glimcher, and R.G. Griffin. 1991. Solid state ^{31}NMR studies of the conversion of amorphous tricalcium phosphate to apatitic tricalcium phosphate. Calcif. Tiss. Int. 49:378–382.

Roch, G.E., M.E. Smith, and S.R. Drachman. 1998. Solid state NMR characterization of the thermal transformation of an illite-rich clay. Clays Clay Miner. 46:694–704.

Rorschach, H.E. 1964. Nuclear relaxation in solids by diffusion to paramagnetic impurities. Physica 30:38–48

Sanders, J.K.M., and B.K. Hunter. 1993. Modern NMR spectroscopy: A guide for chemists. Oxford Univ. Press, Oxford.

Schroeder, P.A., and R.J. Pruett. 1996. Fe ordering in kaolinite: Insights from ^{29}Si and ^{27}Al MAS NMR spectroscopy. Am. Mineral. 81:26–38.

Schroeder, P.A., R.J. Pruett, and V.J. Hurst. 1998. Effects of secondary iron phases on kaolinite ^{27}Al MAS NMR spectra. Clays Clay Miner. 46:429–435.

Steinberg, S.L., D.W. Ming, K.E. Henderson, C. Carrier, J.E. Gruener, D.J. Barta, and D.L. Hennninger. 2000. Wheat responses to differences in water and nutrient status between zeoponic and hydroponic growth systems. Agron. J. 92:353–360.

Sutter, B. 2000. Structural properties and dissolution of iron, manganese, and copper containing synthetic hydroxyapatite. Ph.D. diss. Texas A&M Univ., College Station, TX.

Tripathy, N.K., P.N. Patel, and A. Panda. 1989. Preparation, IR, and lattice constant measurments of mixed (Ca + Cu + Zn) hydroxylapatites. J. Solid State Chem. 80:1–5.

Wu, Y., M.J. Glimcher, C. Rey, and J.L. Ackerman. 1994. A unique protonated phosphate group in bone mineral not present in synthetic calcium phosphate. J. Mol. Biol. 244:423–425.